Phase diagram with an enhanced spin-glass region of the mixed Ising–XY magnet $LiHo_xEr_{1-x}F_4$

J. O. Piatek,[1,*] B. Dalla Piazza,[1] N. Nikseresht,[1] N. Tsyrulin,[1] I. Živković,[2] K. W. Krämer,[3] M. Laver,[4,5] K. Prokes,[6] S. Mataš,[6] N. B. Christensen,[5] and H. M. Rønnow[1]

[1]*LQM, ICMP, Ecole Polytechnique Fédérale de Lausanne, CH-1015 Lausanne, Switzerland*
[2]*Institute of Physics, Biječnika c. 46, HR-10000, Zagreb, Croatia*
[3]*Department of Chemistry and Biochemistry, University of Bern, CH-3012 Bern, Switzerland*
[4]*Laboratory for Neutron Scattering, Paul Scherrer Institut, CH-5232 Villigen, Switzerland*
[5]*Department of Physics, Technical University of Denmark, DK-2800 Kgs. Lyngby, Denmark*
[6]*Helmholtz-Zentrum Berlin für Materialien und Energie, Hahn-Meitner Platz 1, D-14109, Berlin, Germany*

(Received 5 March 2013; published 8 July 2013)

We present the experimental phase diagram of $LiHo_xEr_{1-x}F_4$, a dilution series of dipolar-coupled model magnets. The phase diagram was determined using a combination of ac susceptibility and neutron scattering. Three unique phases in addition to the Ising ferromagnet $LiHoF_4$ and the XY antiferromagnet $LiErF_4$ have been identified. Below $x = 0.86$, an embedded spin-glass phase is observed, where a spin glass exists within the ferromagnetic structure. Below $x = 0.57$, an Ising spin glass is observed consisting of frozen needlelike clusters. For $x \sim 0.3$–0.1, an antiferromagnetically coupled spin glass occurs. A reduction of $T_C(x)$ for the ferromagnet is observed which disobeys the mean-field predictions that worked for $LiHo_xY_{1-x}F_4$.

DOI: 10.1103/PhysRevB.88.014408 PACS number(s): 75.50.Dd, 75.50.Ee, 75.50.Lk

I. INTRODUCTION

When combinations of disorder and frustration are present in a magnetic system, the so-called spin-glass state can arise. In such a state, the long-range order is suppressed, but spins still exhibit spatial and temporal correlations. Over the last 30 years, much theoretical and experimental work has focused on spin glasses, however, materials with a well-defined Hamiltonian are to this day something of a rarity. One candidate for a well-defined spin-glass system has been $LiHoF_4$ diluted with nonmagnetic yttrium.[1–4] The attractiveness of this system stems from the well-described Hamiltonian of the Ising ferromagnet parent compound $LiHoF_4$.[5–8] Many of the interesting phenomena observed in $LiHo_xY_{1-x}F_4$ (Refs. 7 and 9–12) are a direct consequence of the frustrated long-range dipolar interaction between Ho^{3+} moments. The combination of this frustrated interaction and the quenched disorder induced by the random Ho^{3+} population on the rare-earth site make this system a perfect candidate for spin-glass formation. From a theoretical point of view, the Ising anisotropy of the moments decreases the complexity, effectively to a simple anisotropic $s = \frac{1}{2}$ model, allowing for a large number of theoretical predictions to be made.[13–15]

A recent theme in this system is the role of the off-diagonal dipolar terms in the Hamiltonian, the effect of which is tuned by a magnetic field transverse to the Ising axis.[13,14] It was discovered that in the presence of a small transverse field, $LiHo_xY_{1-x}F_4$ is a perfect realization of the classical random field Ising magnet (RFIM).[13,16] One motivation for these studies was experimental nonlinear ac susceptibility data in the presence of a transverse magnetic field, which suggested a $T = 0$ first-order spin-glass quantum phase transition.[3,17] A second group found no evidence of either a classical or quantum spin-glass state.[18] A third group found very strong evidence of a classical spin glass,[19–21] but did not investigate its behavior in the presence a transverse field. On the theoretical side, two independent groups reach the conclusion that the presence of a transverse field induces random fields which destroy true spin-glass order.[13,14,16] Furthermore, it has been demonstrated[13] that the observed nonlinear susceptibility[3] is consistent with this spin-glass-like state.

The key idea of this paper is that introducing Er into the parent compound in place of Y should increase frustration due to the XY anisotropy observed in $LiErF_4$.[22–24] The addition of these off-diagonal terms in the Hamiltonian could drive the onset of glassy behavior up to higher temperatures and extend the range of concentrations where they are visible. Moreover, the resulting compounds are in the class of mixed anisotropy systems, where rich phase diagrams including coexisting magnetic phases have been both theoretically predicted[25–27] and experimentally observed.[28,29] This paper presents ac susceptibility and neutron diffraction studies on $LiHo_xEr_{1-x}F_4$ for 15 concentrations from $x = 1$ to 0. We establish a phase diagram with several striking features compared both to $LiHo_xY_{1-x}F_4$ and to simple mean-field (MF) expectations for $LiHo_xEr_{1-x}F_4$: (a) The spin-glass region is greatly extended, both in terms of x and in temperature, up to a maximum $T_f > 0.5$ K; (b) T_C for ferromagnetic order decreases faster than for Y dilution and in contrast to MF predictions; (c) the antiferromagnetic order found in pure $LiErF_4$ is destroyed by just 10% of Ho.

The experimentally determined phase diagram for $LiHo_xEr_{1-x}F_4$ is shown in Fig. 1. Blue circles indicate the ferromagnetic T_C, green squares the spin glass T_f at 1 kHz, and red diamonds the antiferromagnetic T_N. Additional freezing transitions which occur within a ferromagnetic or spin-glass state are indicated by the light blue and yellow triangles, respectively. The light blue and green ellipses show the range of T_f observed in the frequency range measured for each sample. Moving from large to small x, three phases in addition to the Ising ferromagnet for $LiHoF_4$ and XY antiferromagnet in the case of $LiErF_4$ are observed. Already at $x = 0.86$ at very low temperatures there are indications of some form of spin-glass behavior. The temperature of the onset of the glassy state increases steadily with decreasing x. Once x falls below a critical value, of around $x = 0.57$, the long-range ferromagnetic

 ©2013 American Physical Society

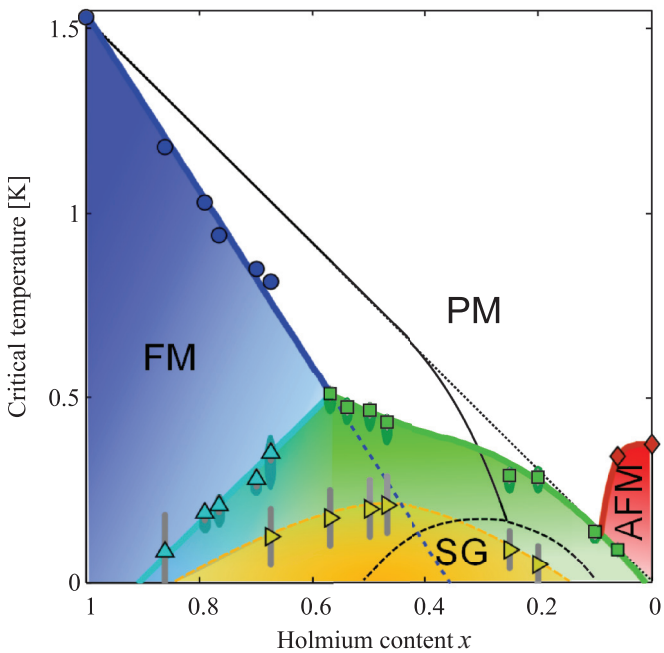

FIG. 1. (Color online) Experimental phase diagram of $LiHo_xEr_{1-x}F_4$ with the phase diagram of $LiHo_xY_{1-x}F_4$ (black line) overlaid to highlight the extended glassy region observed here. Blue circles and red diamonds show, respectively, ferromagnetic (T_C) and antiferromagnetic (T_N) order. Green squares indicate a spin-glass freezing (T_f) from a paramagnetic state. Secondary glasslike transitions from either a ferromagnetic or spin-glass state are shown as light blue and yellow triangles, respectively. The ellipses show the range of T_f in the frequency range measured for each sample (typically 1 Hz to 4 kHz). Lines are guides to the eye.

order is completely suppressed and replaced by a spin-glass phase. The maximum observed T_f is found for $x = 0.57$ and gradually decreases until antiferromagnetic order occurs for $LiErF_4$. The phase diagram for $LiHo_xY_{1-x}F_4$ is shown in black and highlights the extended glassy region observed here.

One challenge in experimental studies of $LiHo_xY_{1-x}F_4$ is the low temperatures of the spin-glass phase at $T \lesssim 150$ mK. This is compounded by the poor thermal conductivity and large specific heat of the samples, which make it difficult at best to be certain of thermal equilibrium. From the details expounded below, it can be seen that extraordinary steps were taken to ensure the thermal equilibrium of our $LiHo_xEr_{1-x}F_4$ samples.

The layout of this paper is as follows. Section II outlines the ac susceptibility experiment and describes the results. Section III discusses neutron diffraction results obtained on samples with $x = 0.79$, 0.5, and 0.25. Both sets of results are interpreted in the framework of mean-field calculations in Sec. IV. The final section is dedicated to discussion of the results in a more general context and conclusions.

II. AC SUSCEPTIBILITY

$LiHo_xEr_{1-x}F_4$ samples were prepared from mixtures of LiF and MF_3 in a 53:47 (Li:M) molar ratio with x the ratio of HoF_3 to ErF_3. The mixture of salts was melted in a glassy carbon Bridgman ampule at a temperature of 880 °C in an inert gas atmosphere. The melt was subsequently slowly cooled over 7 days. The purity of the resulting polycrystals was checked by powder x-ray diffraction and the Ho to Er ratio verified by EDX measurements with an accuracy of ±0.5%.

Small polycrystals of $LiHo_xEr_{1-x}F_4$ were ground to powder and then mixed with Stycast W19 to ensure good thermal contact. The resulting paste was pressed into a 20-mm-long 2-mm-diameter mold and four 200-μm-diameter copper wires were inserted into the mixture which was then baked to cure the Stycast. The copper wires were attached directly to the thermometer housing on the mixing chamber, to ensure the best possible thermalization. Complex ac susceptibility measurements were carried out in an Oxford Kelvinox 25 dilution refrigerator, using coaxially compensated mutual inductance coils. The primary coils are supplied with an ac current using a Keithley 6221 ac current source and the signal induced in the secondary coils is measured using a Signal Recovery 7265 lock-in amplifier. The measurements used an ac excitation current of 10 μA, corresponding to a field of 42 mOe, in the range of 1 Hz–4 kHz.

Before looking at the results in detail, some concepts related to spin glasses must be introduced. The spin-glass state is typically characterized by a sharp cusp in the real signal of the ac susceptibility, around the freezing temperature T_f, which is rounded out by the smallest fields.[30] In the case of insulating spin glasses, the imaginary susceptibility is dominated by the spin-glass dynamics. χ'' begins to increase at $T > T_f$, has an inflection point which coincides with the peak in χ', and peaks shortly afterwards before dropping down to zero at low temperatures. The temperature at which the χ' cusp occurs depends on the frequency of the ac driving field, as correlated spins in different local environments with different relaxation times will freeze-out at different temperatures. The frequency dependence of T_f is logarithmic for almost all experimentally accessible frequencies (10^{-3}–10^{10} Hz) and can be well described by an Arrhenius law:

$$f = 1/\tau_{\text{char}} = f_0 \exp(-E_a/k_B T), \tag{1}$$

where E_a and f_0 are the energy barrier and characteristic frequency in the case of a superparamagnet. One way of separating a superparamagnet, where spins form noninteracting clusters, from a spin glass, which contains long-range correlations, is by looking at the frequency sensitivity of $T_f(f)$ (Refs. 31 and 32):

$$\mathcal{K} = \frac{\Delta T_f}{T_f \Delta \log_{10}(f)}. \tag{2}$$

Generally, metallic canonical spin glasses have values of $\mathcal{K} \leqslant 0.01$, insulating spin glasses have values in the region $0.01 \leqslant \mathcal{K} \leqslant 0.1$, and shifts higher than this are typical of superparamagnets.

An alternate explanation of the frequency dependence of T_f is that of a critical scaling law associated with a spin-glass phase transition at finite temperature T_g. This explanation was introduced when a divergence from Arrhenius law was observed at $T_f \to T_g$ in some spin-glass systems.[33] The critical scaling is usually expressed as[34]

$$\tau = \tau_0 (T/T_g - 1)^{-z\nu}, \tag{3}$$

where τ is the characteristic spin relaxation time at temperature T, T_g is the glass temperature, and the product

$z\nu$ is the dynamical exponent. This form of dynamical scaling is supported by calculation on Ising spin-glass models, where Monte Carlo simulations[35,36] find critical scaling with $z\nu \approx 7$. Care should be taken when referring to the different freezing temperatures T_f and T_g; T_f is the frequency-dependent temperature at which the spin-glass transition is observed, whereas T_g is the zero-frequency spin-glass transition temperature. As will be demonstrated, it can be difficult to distinguish between these two dynamical situations in the range of experimentally accessible frequencies. A final complication in $LiHo_xEr_{1-x}F_4$ is the large anisotropy of the Ising moments which can prevent the system reaching equilibrium, resulting in a thermally activated spin glass.[37]

An overview of the real $\chi'(T)$ and the imaginary $\chi''(T)$ components of the complex ac susceptibility is presented for selected compositions in Fig. 2. Starting from large x, a frequency-independent peak in χ' and concomitant onset of χ'' is seen just below 1 K, which we will later show to be ferromagnetic order. At lower temperatures, there is a frequency-dependent drop in χ' which appears to correspond to a peak in χ''. As x decreases, T_C decreases linearly with x down to $x = 0.57$, where long-range order is no longer observed. The peak in χ' broadens and the temperature of the peak now depends on frequency, indicating a slowing down process consistent with a spin-glass state. This frequency-dependent peak continues all the way down to $x = 0.1$, with the features in the susceptibility constantly evolving with x.

A. Ferromagnetic region

We illustrate the analysis of the ferromagnetic region in detail for $x = 0.675$ in Fig. 3, which shows susceptibility curves taken at 7.7, 77, and 770 Hz. At $T = 0.815$ K, there is simultaneously a peak in χ' (top panel) and a kink of χ'' (bottom panel). This is a clear indication of a ferromagnetic transition where χ' diverges and domain-wall motion causes a sudden increase in χ''. This high-temperature behavior is essentially the same behavior as observed for $LiHoF_4$,[6] with the exception that T_C has now decreased to lower temperatures. At lower temperatures, there is a clear frequency-dependent behavior in both $\chi'(T)$ and $\chi''(T)$. The frequency-dependent peak observed in χ'' just below T_C is probably due to domain-wall motion in the ferromagnet. The lower-temperature peak in χ'' at temperatures around 250 mK is likely due to the freezing-out of moments not in the ferromagnetic state.

To better determine the behavior of the frequency-dependent features, we note that the presence and dynamics of domain walls in the sample, inferred from the peak χ'' just below T_C, will give rise to a signal in χ'. The observed χ' is therefore considered to be the superposition of two physically distinct phenomena, a high-temperature signal from the ferromagnet and a low-temperature signal from a spin glass. The ferromagnetic component of the susceptibility is estimated by fitting the data with an exponential function in the temperature range where the signal from the freezing is assumed to be negligible (in this case 0.03 K $< T <$ 0.075 K and 0.6 K $< T <$ 0.86 K). Subtracting the fitted component from the measured susceptibility reveals a signal believed to be coming from the spin glass (middle panel), which peaks at roughly the same position as the inflection point of χ'', as is expected for a typical spin glass.

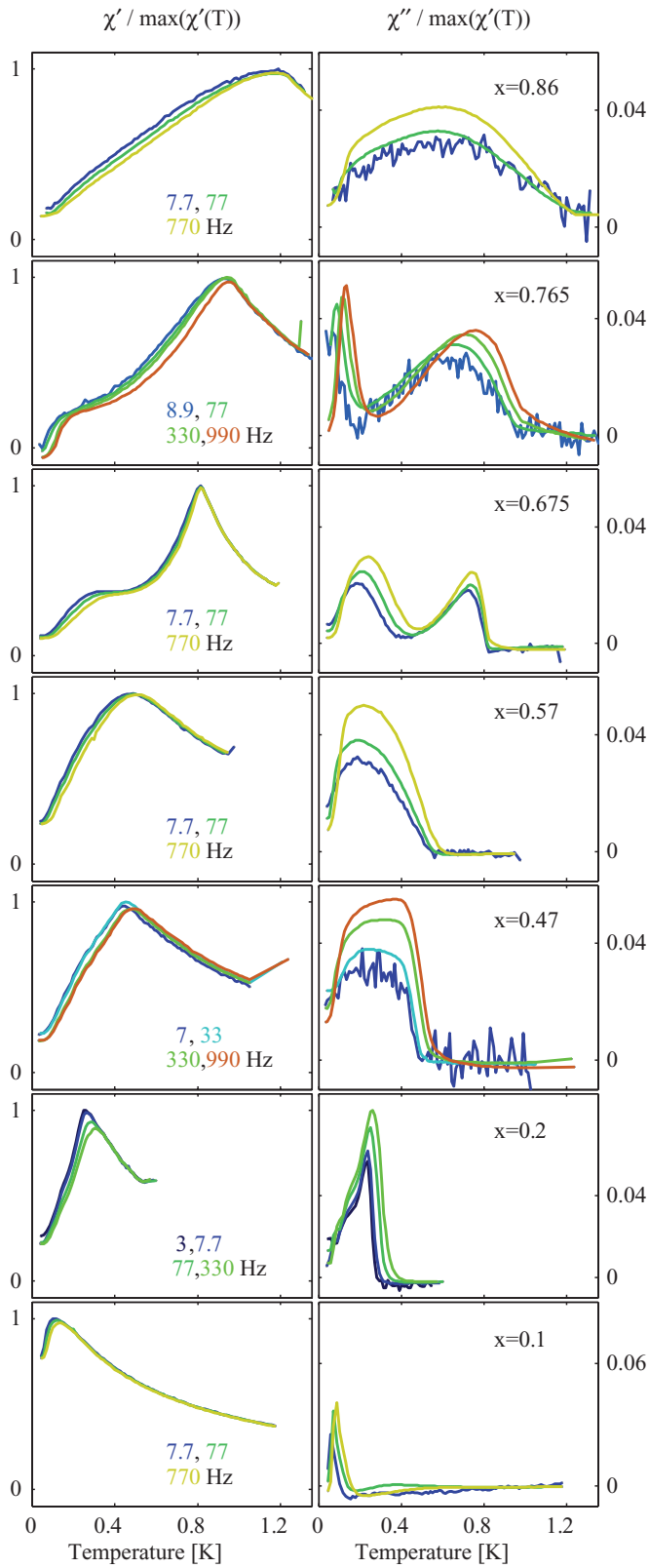

FIG. 2. (Color online) ac susceptibility data for $LiHo_xEr_{1-x}F_4$. Moving from high to low x, the ferromagnetic peak is suppressed by the additional Er content, disappearing completely at $x = 0.57$. Frequency-dependent behavior is seen in all samples, in the form of an embedded spin glass for $0.68 < x \lesssim 0.9$ and more typical spin glasses for $x < 0.57$.

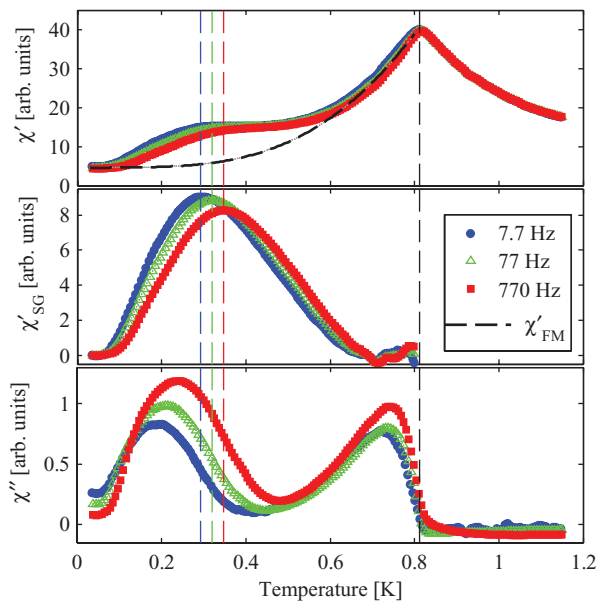

FIG. 3. (Color online) Temperature scans of $LiHo_{0.675}Er_{0.325}F_4$ taken at 7.7, 77, and 770 Hz. The peak in χ' at 0.815 K is T_C of the ferromagnetic long-range order, and the frequency dependence seen at $T = 0.2$–0.4 K corresponds to a spin-glass transition. T_f is determined by subtracting a ferromagnetic background signal (dashed line) from the measured curve, leaving the usual peak in the susceptibility (middle panel).

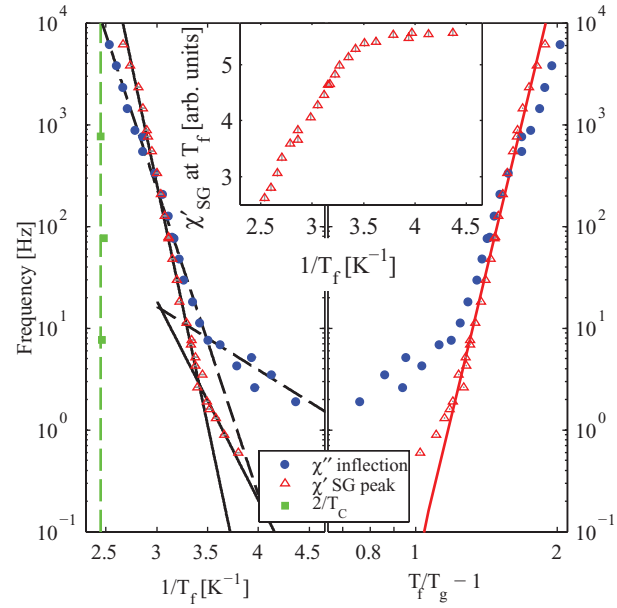

FIG. 4. (Color online) Left: Frequency dependence of T_f for $x = 0.675$ with a fit to the Arrhenius law. Comparison of the frequency dependence of T_f if determined by the inflection point before the peak in χ'' or the peak in χ' after subtraction of the background signal from the ferromagnet. To demonstrate the frequency independence of $T_C = 0.815$ K, $2/T_C$ is also plotted. Right: Scaling law for the same data sets assuming a zero-frequency glass transition temperature T_g. The inset shows the temperature dependence of the χ'_{SG} peak amplitude.

The frequency dependence of T_f is traditionally compared to either an Arrhenius law or a scaling law.[30] Avoiding prejudice between these two paradigms for spin glasses, we show in the left panel of Fig. 4 an Arrhenius-type plot and in the right panel a scaling-law plot. In order to carry out the scaling-law analysis in a reproducible fashion, the value of T_g must be determined and fixed. As there is no clear indication of a low-frequency saturation in T_f, T_g is determined by fitting Eq. (3) for the entire possible range of T_g $[0 < T_g < T_f(\min)]$. The trial temperature which gives the best fit to this equation is assumed to be the zero frequency T_g. The figure shows the dynamics of T_f as extracted from the inflection point in χ'' (blue circles) and from peak in χ' (red triangles) revealed by subtracting the ferromagnetic component. To illustrate the frequency independence of T_C, the green squares show $2/T_C$.

Focusing first on the Arrhenius plot, a value of $\mathcal{K} = 0.02$ is extracted for the high-temperature (and high-frequency) region. The extracted value of the attempt frequency $f_0 = 4 \times 10^{10}$ Hz gives an indication that the dynamics could be well described by an Arrhenius law. At lower temperatures and longer time scales, the Arrhenius behavior is lost and it appears that the system crosses over into a different set of dynamics, which can be explained with a new Arrhenius law with $\mathcal{K} = 0.04$. An examination of the peak in the real susceptibility (inset of Fig. 4) also points towards an underlying change in behavior; the peak amplitude becomes temperature independent at the same temperature of the crossover in slope. The dynamics can be equally well explained by critical scaling, with $T_g = 0.13 \pm 0.002$ K, $\tau_0 = 3.5 \pm 0.5$ s, and $z\nu = 19 \pm 0.5$. The very large values of τ_0 and $z\nu$ coupled with the low-temperature deviation from the fit seem to imply that the system does not follow a dynamic scaling law.

B. Large-*x* spin-glass region

As x is decreased further, the ferromagnetic order disappears completely, and the system shows very broad frequency-dependent features. Given the relatively similar amounts of Ho and Er, and the behavior of the large-x phase, it seems plausible that there are in fact two transitions which constitute the broad signal.

In the case of $x = 0.50$, the susceptibility has been measured on single crystals in addition to the powder samples. Given the very high anisotropy of both Ho and Er moments and their different nature, it is possible to partially separate their contributions, as χ_{zz} is predominantly sensitive to the Ising moments of Ho and χ_{xx} predominantly sensitive to the XY Er moments. A comparison of these two susceptibilities is shown in Fig. 5. The susceptibilities measured along different crystallographic directions show strikingly different behavior. At $T = 0.450 \pm 0.02$ K, χ' peaks in both measurements, with the peak position depending on the frequency of the measurement, indicating the freezing of the moments. Below this temperature, χ_{zz} decreases relatively quickly, as expected for an Ising spin glass, whereas χ_{xx} remains relatively broad and does not decrease significantly. The imaginary component of the susceptibility shows similar differences, where two frequency-dependent peaks are clearly visible in χ''_{xx}.

As was the case for $x = 0.675$, the frequency dependence of T_f is fitted both by Arrhenius activated dynamics and critical scaling, as shown in Fig. 6. There is a low-temperature deviation from Arrhenius dynamics in the opposite direction to the $x = 0.675$ sample; in this case the freezing temperature tends towards a zero-frequency value. This is reflected in the

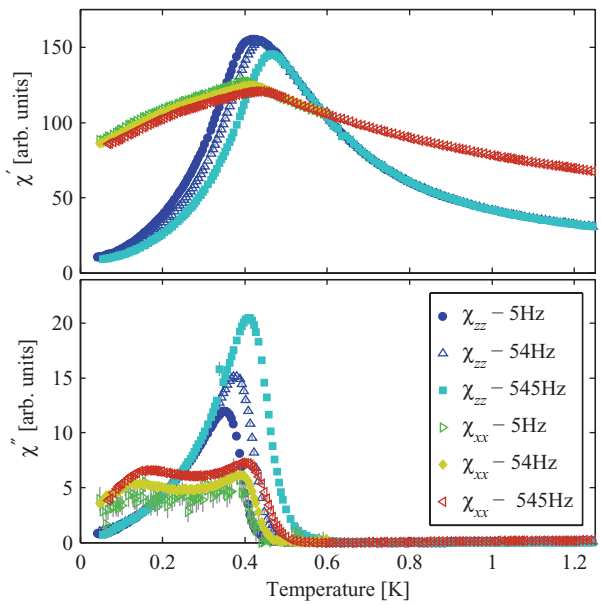

FIG. 5. (Color online) Temperature scans of single crystals of $LiHo_{0.50}Er_{0.50}F_4$ comparing χ_{zz} and χ_{xx}. In order to better compare the two data sets, χ'_{xx} has been scaled by a factor of 20 and χ''_{xx} by a factor of 50.

critical scaling dynamics, where there is no visible deviation from the expected fit. The large value of $f_0 \approx 10^{20}$ Hz would be a further argument that the system undergoes a true spin-glass phase transition and is therefore described by critical scaling dynamics. The lowest-temperature peak in χ''_{xx} is believed to be due to a second glass transition, whose freezing temperature is taken as the peak in susceptibility. As the peak is small compared to the background signal, it is only possible to

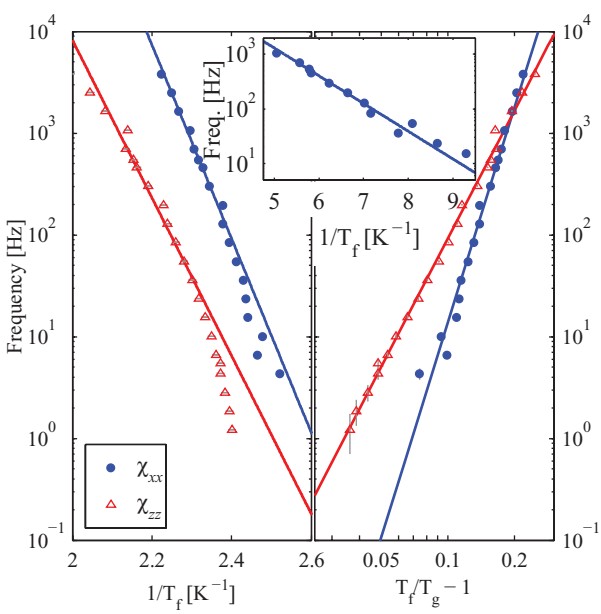

FIG. 6. (Color online) Frequency dependence of T_f in $LiHo_{0.50}Er_{0.50}F_4$ expressed in terms of (left) Arrhenius behavior and (right) a dynamic scaling law. The inset shows the frequency dependence of the low-temperature peak in χ''_{xx} in the range of frequencies where the peak was extractable.

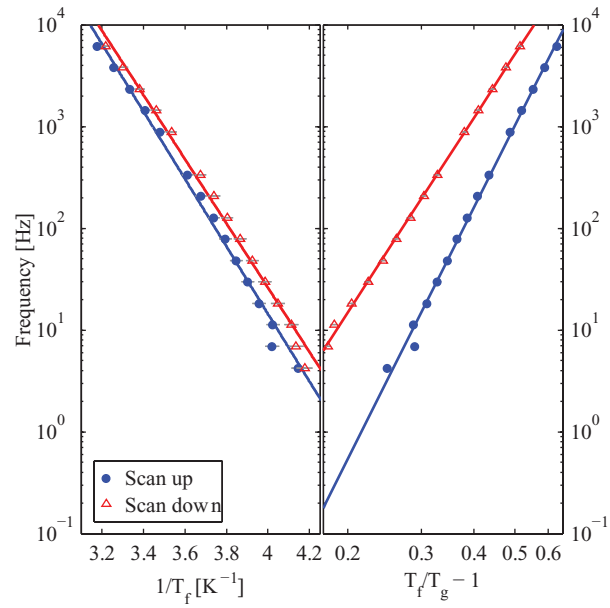

FIG. 7. (Color online) Frequency dependence of T_f in $LiHo_{0.25}Er_{0.75}F_4$ expressed in terms of (left) Arrhenius behavior and (right) critical scaling. The data compare T_f extracted from scans ramping both up and down in temperature, which are offset by 5 mK, probably due to thermalization issues.

extract T_f between 10 and 1000 Hz. In this frequency range, the dynamics are well explained by an Arrhenius law, as can be seen in the inset of Fig. 6.

C. Small-x spin-glass region

As x decreases further, the spin-glass freezing temperature continues to slowly decrease and the features in the susceptibility sharpen. At $x = 0.25$ the susceptibility has sharpened to the point that both χ' and χ'' resemble those found in typical spin glasses.[30] The frequency dependence of this sample is shown in Fig. 7, which plots the dependence of T_f taken for temperature scans when ramping either low to high temperatures (blue circles) or from high temperatures to low ones (red triangles). The difference between the two scans gives an idea of the maximum offset due to insufficient thermalization, which is found to be on the order of 5 mK. In this sample, both Arrhenius and critical scaling dynamics produce fits of equal quality, with no clear variation from either law immediately visible. A comparison of the relevant parameters from the Arrhenius and critical scaling fits does not shed any more insight into the nature of the dynamics in this compound; both are within the expected ranges for the respective fit type.

All of the samples measured have been analyzed in a similar manner to these three examples, with the data being used to build up the phase diagram shown in Fig. 1. The parameters relating to the phase transitions T_C, $T_{f(1\,\mathrm{kHz})}$, and T_g and dynamics $\mathcal{K}$, $z\nu$, and τ_0 have been extracted and are summarized in Table I.

III. NEUTRON SCATTERING

Neutron scattering measures the correlation function of the moments, therefore complementing the ac susceptibility

TABLE I. Summary of transition temperatures and spin-glass parameters related to dynamics in $LiHo_xEr_{1-x}F_4$. All temperatures are in Kelvin.

x	T_c	T_f (1 kHz)	f_0 (Hz)	$\mathcal{K}$	T_g	$z\nu$	τ_0 (s)
1	1.53	N/A	N/A	N/A	N/A	N/A	N/A
0.860	1.20	0.083	4×10^5	0.077			
0.790	1.04	0.191	4×10^8	0.044	0.043	12.9	1.3×10^3
0.765	0.95	0.197	2×10^{11}	0.080	0.174	2.2	1.6×10^{-6}
0.700[a]	0.85	0.280	2×10^{15}	0.025	0.156	10	1.3×10^{-5}
0.675	0.815	0.347	4×10^{10}	0.027	0.130	19	3.5
0.570	N/A	0.510	5×10^{34}	0.024	0.430	9.0	6.2×10^{-11}
0.540	N/A	0.474	3×10^{20}	0.046	0.396	6.4	4.3×10^{-9}
0.500[b]	N/A	0.471	4×10^{19}	0.049	0.405	4.1	1.5×10^{-7}
0.500[a]	N/A	0.437	1×10^{24}	0.042	0.369	7.0	1.0×10^{-9}
0.470	N/A	0.434	2×10^{20}	0.054	0.299	6.2	6.4×10^{-9}
0.250	N/A	0.288	3×10^{13}	0.069	0.199	8.2	3.7×10^{-7}
0.200	N/A	0.286	3×10^{13}	0.070	0.196	7.5	4.2×10^{-7}
0.100	N/A	0.138	3×10^{11}	0.080	0.079	8.6	1.3×10^{-5}
0.060	0.342	(0.15)					
0	0.375	N/A	N/A	N/A	N/A	N/A	N/A

[a]Single-crystal measurements of χ_{xx}.
[b]Single-crystal measurements of χ_{zz}.

measurements which measure the spatially averaged dynamics of the system. In particular, neutron scattering allows for the determination of spatial correlations and the directions of the magnetic moments involved in the spin-glass state. Furthermore, neutron scattering can be used to discern whether the correlations between moments are ferromagnetic or antiferromagnetic in nature.

Neutron scattering measurements have been carried out on three samples, with $x = 0.79$, 0.5, and 0.25. Due to the poor thermal conductivity of the $LiMF_4$ compounds, particular care has been taken in ensuring the best possible thermal conductivity. Large single crystals were cut into thin slices roughly 1.5 mm thick and individually gold sputtered creating a layer 2–3 μm thick. These blades were then placed inside a solid walled box made from a single piece of oxygen-free high conductivity (OFHC) copper, with a thin copper foil strip placed between each blade. The copper foil strips are attached to the sample holder and a lid is screwed on to the box, pressing the blades together and thus ensuring a good thermal contact. In the case of $x = 0.25$, ac susceptibility was measured *in situ* during the neutron scattering experiment using a homemade split coil ac susceptometer. Figure 8 shows a picture of the mounted sample holder for this experiment (right) and a preliminary sample holder (left), where the configuration of the blades of crystal is clearly visible. For the measured sample, the central blade was cut 10 mm longer than the rest, and the split coil susceptometer was placed on either side of this protrusion to measure the ac susceptibility.

A. Ferromagnetic region

Measurements on $x = 0.79$ were carried out on the E4 thermal neutron diffractometer at HZB in Germany on five blades cut from a single crystal with total dimensions of $5 \times 5 \times 30$ mm. The sample was placed inside a dilution fridge and vertical-axis superconducting magnet, allowing for temperatures down to 50 mK and fields up to 5 T. The field direction was perpendicular to the c axis along the $(h\bar{h}0)$ direction in order to study the possible transverse field Ising model (TFIM) quantum phase transition. The scattering plane was the $(hh0)$-$(00l)$ plane and the incoming beam of neutrons was monochromated to a wave vector of $k_i = 2.59$ Å^{-1}.

The long-range ferromagnetic order has been confirmed by measuring the temperature dependence of the (2,2,0) and

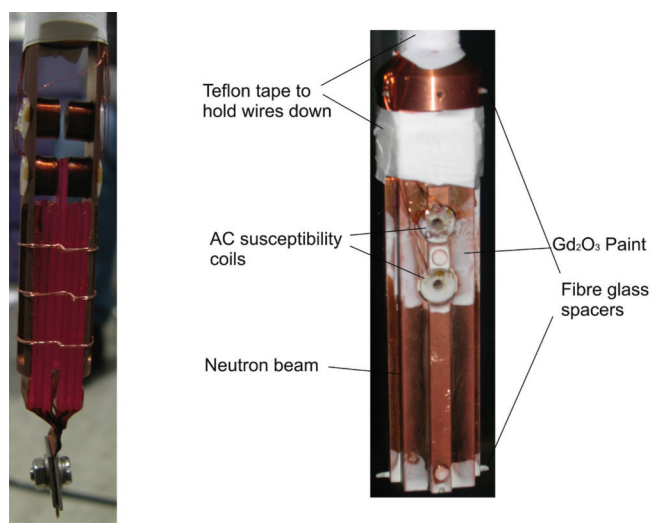

FIG. 8. (Color online) Photo of the sample holder used for the measurements on $LiHo_{0.25}Er_{0.75}F_4$. Left: Preliminary sample holder showing the configuration of the individual blades in the sample holder. Right: Sample holder used for experiments made from a single piece of OFHC copper. Each blade has been sputtered with gold and thermalized to the sample holder via a 12 mm $\times$ 25 μm copper foil. The central blade was cut 10 mm longer than the others and sits inside a split-coil susceptometer to allow for *in situ* measurements of ac susceptibility.

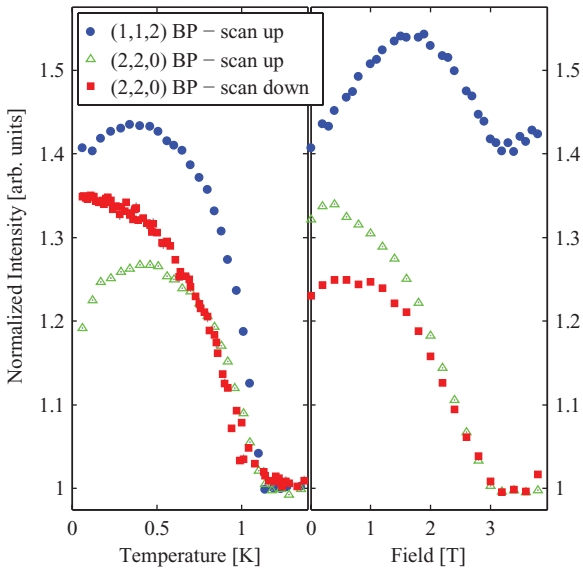

FIG. 9. (Color online) Temperature (left) and field dependence (right) of the (2,2,0) and (1,1,2) Bragg peaks in $LiHo_{0.79}Er_{0.21}F_4$, indicating the presence of long-range ferromagnetic order. The data have been normalized to the nuclear Bragg peak intensity and the magnetic scattering from the (1,1,2) Bragg peak has been scaled down by a factor of 5 relative the (2,2,0) Bragg peak.

(1,1,2) nuclear Bragg peaks, shown in the left panel of Fig. 9. The scan up is measured after having been at high field, so can therefore be thought of as a high-field-cooled (HFC) state, whereas the scan down is a zero-field-cooled (ZFC) state. As T drops below T_C, the intensity of the Bragg peak begins to increase, indicating the buildup of ferromagnetic order. The Bragg peak could be fitted using a resolution-limited Gaussian line shape, which indicates that the ferromagnetic correlations are long ranged. There is also a hysteresis between the HFC and ZFC states and the ordered moment in the ferromagnet is permanently reduced by being at large transverse fields.

The field dependence of the ferromagnetic signal has also been measured for these two Bragg peaks and is shown in the right panel of Fig. 9. For the (2,2,0) Bragg peak, the picture is relatively simple: the application of the transverse field gradually destroys the long-range ferromagnetic order. The (1,1,2) peak intensity first increases, then decreases, and finally increases above H_C. This behavior is likely a combination of the spins being polarized by the field (increasing intensity) and destruction of the c-axis correlations (decreasing intensity). Such behavior is not seen in the (2,2,0) Bragg peak as the moments are polarized parallel to the scattering vector and as such have a vanishing cross section.

B. Large-x spin-glass region

Measurements on both the $x = 0.50$ and 0.25 samples were carried out on the cold neutron triple axis spectrometer RITA-II at PSI in Switzerland. For $x = 0.50$, the sample had total dimensions of $12 \times 12 \times 40$ mm and was mounted in a vertical field superconducting magnet and dilution fridge. The scattering plane was the (h00)-(00l) plane, the magnetic field was aligned along the b axis. The incoming neutrons along with

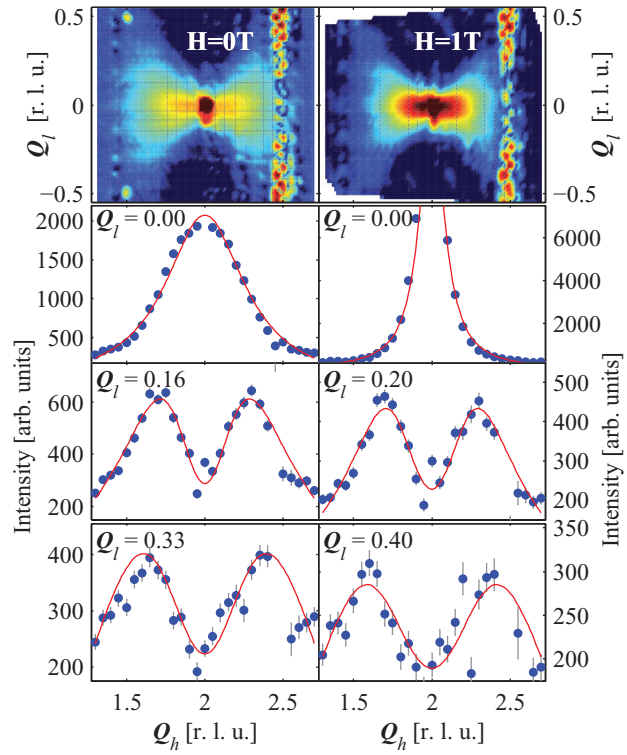

FIG. 10. (Color online) Top: $\boldsymbol{Q}$-dependent scattered intensity centered around the (2,0,0) Bragg peak at 50 mK and 0 T (left), 1 T (right). The scans show a butterfly shape scattering typical for dipolar coupled Ising moments, with the spin-spin correlation length increasing at 1 T. Lower panels: $\boldsymbol{Q}_h$ scans across the diffuse scattering for selected $\boldsymbol{Q}_l$ after subtraction of 3 T background to remove copper and aluminum powder lines (these are the origin of the streaks at $\boldsymbol{Q}_h \sim 2.6$ in the top panels). The data are subsequently fit to Eqs. (4) and (5).

the analyzer blades were tuned to a wave vector $k_i = 1.97$ Å^{-1}. The measurements were carried out using all analyzer blades in the so-called *monochromatic imaging mode*, where each analyzer detects a slightly different $\boldsymbol{Q}$ vector[38] to measure out a region of $\boldsymbol{Q}$ space centered around the (2,0,0) Bragg peak. This region has been mapped out at base temperature, both in zero field and in a 1 T transverse field as shown in Fig 10.

In the top two panels, the $\boldsymbol{Q}$-dependent scattered intensity is seen to have a butterfly shape distribution, as is expected for the critical scattering of dipolar coupled Ising moments.[39] When a transverse field of 1 T is applied, the pattern narrows and increases in intensity near the center, indicating an increase in the spin-spin correlation length. The lower panels show $\boldsymbol{Q}_h$ scans taken at selected $\boldsymbol{Q}_l$.

An analytical expression for the magnetic cross section of Ising moments in the quasielastic limit is[40]

$$\frac{d\sigma}{d\Omega} \propto \left[1 - \left(\frac{\boldsymbol{Q}_z}{\boldsymbol{Q}}\right)^2\right] f^2(\boldsymbol{Q}) \frac{\chi(\boldsymbol{Q},T)}{\chi^0(T)}, \tag{4}$$

where z indicates the Ising direction, $f(\boldsymbol{Q})$ is the magnetic form factor of Ho^{3+}, $\chi(\boldsymbol{Q},T)$ is the wave vector and temperature-dependent susceptibility, and $\chi^0(T)$ is the single-ion susceptibility of the system. If we consider $\boldsymbol{q} = \boldsymbol{Q} - \tau$, the deviation of $\boldsymbol{Q}$ from the (2,0,0) reciprocal lattice vector, then

renormalization-group theory for a uniaxial, dipolar-coupled system gives[41]

$$\frac{1}{\chi(\boldsymbol{Q},T)} \propto 1 + \xi^2\left[\boldsymbol{q}^2 + g\left(\frac{\boldsymbol{q}_z}{\boldsymbol{q}}\right)^2\right], \tag{5}$$

where ξ is the in-plane correlation length and g is an anisotropy factor. The $\boldsymbol{Q}_h$ scans shown in Fig. 10 have been fit to this form of scattering while allowing both ξ and g to vary. Before the fit was carried out, powder lines from the copper sample holder and aluminum cryostat (these are the origin of the streaks at $\boldsymbol{Q}_h \sim 2.6$ in the top panels) were removed from the measured signal. This was done by subtracting a $\boldsymbol{Q}_h$ scan centered around $\boldsymbol{Q} = (2,0,0)$ taken at 3 T from the data. In zero field, a correlation length of $\xi = 16 \pm 1$ Å and an anisotropy factor of $g = 3.3 \pm 0.5$ Å^{-2} are found. When the transverse field is applied, the in-plane correlation length increases to $\xi = 49 \pm 4$ Å and the anisotropy factor increases to $g = 32 \pm 5$ Å^{-2}. This implies that not only are the clusters growing in size in the field, but their geometry is changing and they are becoming relatively wider.

C. Small -*x* spin-glass region

Measurements on the $x = 0.25$ composition were carried out in a dilution fridge and a 1.8 T horizontal magnet along the a axis and scattering neutrons in the (h00)-(00l) plane. Scans were performed around the nuclear extinct (1,0,0) position along with the (2,0,0) Bragg peak to search for, respectively, antiferromagnetic and ferromagnetic order and are shown in Fig 11. The scans were taken at the following fields and temperatures: 1 K and 0 T, 180 mK and 0 T, 180 mK and 1 T, and finally 180 mK and 0 T.

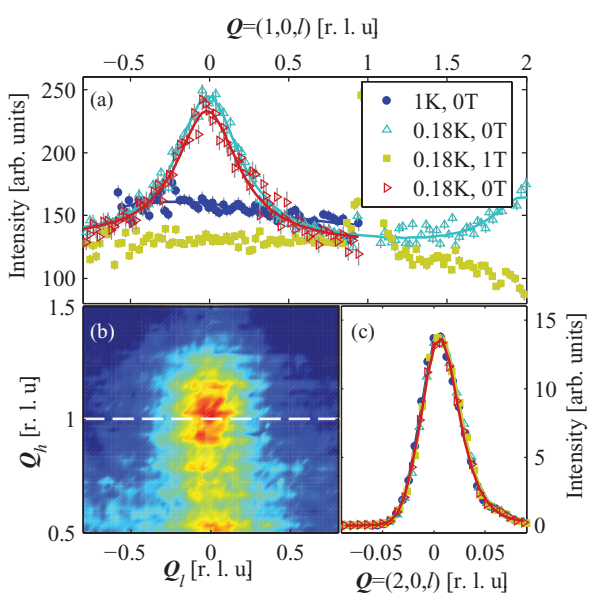

FIG. 11. (Color online) Neutron scattering data on $LiHo_{0.25}Er_{0.75}F_4$. (a) $\boldsymbol{Q}_l$ scans around the (100) forbidden reflection, showing a broad Lorentzian component, corresponding to a spin-spin correlation of $\xi = 44 \pm 2$ Å along the c axis. (b) $\boldsymbol{Q}$-space intensity distribution of this scattering indicating a slight anisotropy with an a-axis correlation length of $\xi = 13 \pm 1$ Å along the a axis. (c) $\boldsymbol{Q}_l$ scans around the (2,0,0) Bragg peak clearly indicating an absence of ferromagnetic correlations.

The scans centered around the (2,0,0) Bragg peak position remain both temperature and field independent, indicating that there is no ferromagnetic order in the system. Centered around the (1,0,0) position, on the other hand, is a very broad and relatively intense Lorentzian signal. If an exponential decay of correlations is assumed, then the correlation length is simply the half width half maximum of this Lorentzian:

$$I \propto \frac{1}{1 + \boldsymbol{Q}^2\xi^2}. \tag{6}$$

The fit is made by first subtracting the high-field signal and second by assuming that the increase in intensity at $\boldsymbol{Q} = (1,0,2)$ is due to the same antiferromagnetic correlations and therefore a Lorentzian with a different amplitude but the same width. Applying this fit yields a c-axis correlation length of $\xi = 44 \pm 2$ Å. The pseudocolor map in panel (b) shows the $\boldsymbol{Q}$ dependence of this scattering and similar analysis results in an a-axis correlation length of $\xi = 13 \pm 1$ Å. Taken together, these two pieces of information indicate elliptical regions of correlated moments containing around 30 rare-earth sites.

The field and temperature dependencies of the spin glass were determined by measuring the scattered intensity at $\boldsymbol{Q} = (1,0,0)$ while ramping the field and temperature, respectively. The ac susceptibility measurements were carried out *in situ* simultaneously during the field and temperature scans. For the temperature scans, the temperature was ramped with the following ramping rates: 17 μK/s for 50 mK $< T <$ 500 mK and 42 μ K/s for 500 mK $\leqslant T <$ 1 K. The temperature scan is presented in the left side of Fig. 12 and the field scan on the right side.

Temperature scans show a continuous decrease in spin-spin correlations which fall off quickly up to ~0.4 K after which they decrease more slowly (top panel). The crossover at 0.4 K

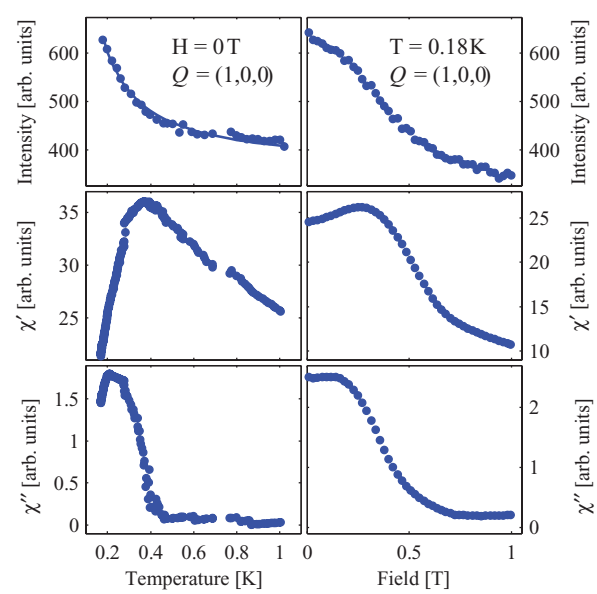

FIG. 12. (Color online) Zero-field temperature dependence (left) and field dependence at 180 mK (right) of the $\boldsymbol{Q} = (100)$ scattered intensity and simultaneously measured ac susceptibility of $LiHo_{0.25}Er_{0.75}F_4$.

coincides with the onset of χ'', and the peak in χ', which gives T_f, occurs at a lower temperature. The rather high temperature where spin-spin correlations increase suddenly can be explained by the THz frequency scale of the neutrons and the logarithmic frequency dependence of T_f. A quick calculation assuming an Arrhenius dependence up to the THz range and using T_f and $\mathcal{K}$ from Table I finds a T_f(1 THz) $\sim$ 0.5 K. In the field scan, the intensity once again drops off continuously. A kink in neutron intensity appears at the same field as the peak in χ''.

IV. DISCUSSION

The rich phase diagram of $LiHo_xEr_{1-x}F_4$ is an ideal playground for the study of spin-glass materials. Like in $LiHo_xY_{1-x}F_4$, by substituting holmium, first the Curie temperature of the ferromagnet is decreased. At lower temperatures a spin-glass state emerges, effectively inside of a ferromagnetic matrix. As x is decreased further, at around $x = 0.6$ the ferromagnetism is completely suppressed and replaced by a spin-glass state showing broad features in the ac susceptibility. As x decreases towards zero, the features in the ac susceptibility sharpen and have the allure of a canonical-like spin glass. Each of these distinct regions of the phase diagram are discussed in detail in the following paragraphs.

A. Ferromagnetic region

Upon first inspection, for large x the system appears to be a good example of a reentrant spin glass, where the spin-glass state is entered not from a paramagnet but from a ferromagnetic phase. The neutron scattering results on $x = 0.79$ indicate that the ferromagnetic state persists down to 50 mK, implying the system is perhaps better described as an *embedded spin glass*, where the spin glass coexists with the ferromagnetic order.

In general, the frequency dependence of this spin-glass-like state does not seem to be well described by either Arrhenius or critical scaling dynamics. In both cases, the extracted parameters seem to vary dramatically from one concentration to the next. In the case of critical scaling, the parameters are very far from those expected from a typical spin glass. For the Arrhenius fits, the low values of f_0 appear to indicate that the entities freezing out are clusters rather than individual spins. This seems somewhat unlikely as cluster size seemingly increases as Er content decreases, but could be due to the spins existing with a long-range ordered matrix.

This embedded spin-glass state shares some similarities with the *antiglass* state observed in $LiHo_{0.045}Y_{0.955}F_4$.[42] More specifically, in both compounds there is a clear deviation from Arrhenius law behavior of the spin-glass freezing temperature, but with no evidence of a zero-frequency freezing temperature.

The ferromagnetic Curie temperature T_C decreases linearly and more rapidly than in $LiHo_xY_{1-x}F_4$. Virtual crystal mean-field (VCMF) calculations fail to capture this effect, giving a $T_C(x)$ *larger* than in $LiHo_xY_{1-x}F_4$, as can be seen in Fig. 13. Given the success of mean-field theory to explain the phase diagram of $LiHo_xY_{1-x}F_4$, this failing is somewhat surprising. Inhomogeneous mean-field (iMF) calculations on a lattice of $100 \times 100 \times 100$ unit cells gives identical results to the VCMF, implying the effect is not simply due to the disorder in

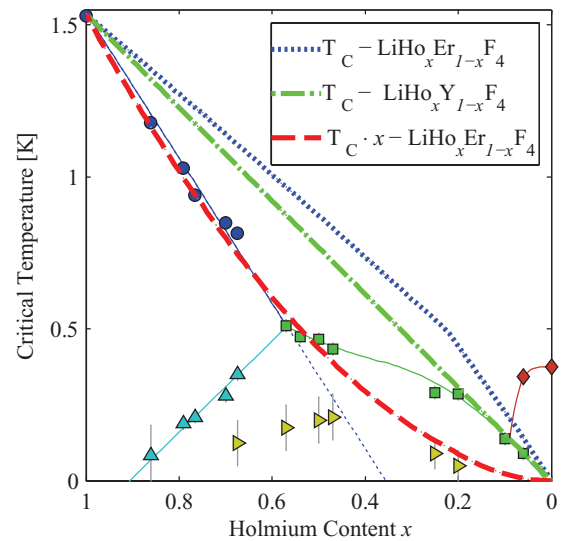

FIG. 13. (Color online) Experimental phase diagram of $LiHo_xEr_{1-x}F_4$ compared with VCMF calculations (blue dotted line). As a reference, the VCMF result for $LiHo_xY_{1-x}F_4$, which is in good agreement with experiments, is shown (green dashed-dotted line). It appears that multiplying T_C found by VCMF additionally by the Ho content x yields good agreement with the experimental phase diagram (red dashed line).

the location of magnetic moments and confirming the system is no longer mean field. In investigating this reduction of $T_C(x)$, we came across an interesting result. If the $T_C(x)$ obtained from mean field is multiplied with an additional x, then there is a remarkably good agreement with the experimental phase diagram as seen in Fig. 13. For the time being, we have no theoretical argument that this is more than a coincidence, although it could prove a useful starting point for additional theoretical work.

Further calculations to explain the rapidly decreasing T_C have been carried out. First, the Hamiltonian containing only the two lowest crystal-field levels was diagonalized for a small cluster of 8 Ho ions surrounding a central Er ion (4 nearest neighbors, 4 next-nearest neighbors) in the presence of the temperature-dependent mean field generated in pure $LiHoF_4$. These calculations gave identical results to the mean-field ones: the Er becomes polarized by the Ho ions, increasing T_C. Similar calculations using the full Hamiltonian were carried out for an Er ion with 4 nearest-neighbor Ho ions, giving the same result. As there is a slight change in lattice parameters for $LiHoF_4$ and $LiErF_4$, on the order of 0.5%, another possibility is that the distorted lattice could influence the crystal-field levels. To investigate this hypothesis, point charge crystal-field calculations were carried out for a variety of symmetrical lattice distortions and the resulting crystal field used in VCMF calculations. The net effect of the distortions was a change in T_C far too small to explain the experimental data.

More theoretical work must be carried out in order to understand the dependence of T_C as a function of Er content. It is clear from the calculations already carried out that it is not a local quantum or classical effect and therefore probably a long-range effect. Given the success of classical Monte Carlo simulations[43,44] in explaining the non-MF behavior observed

in $LiHo_xY_{1-x}F_4$ for $x < 0.5$, these calculations may shed more light on the situation.

B. Large-x spin-glass region

As x decreases, the ferromagnetic component in the χ' disappears completely. In χ'', on the other hand, the peak due to the spin glass begins to widen. Given the existence of a spin glass embedded within the ferromagnetic state for larger x, it seems likely that this widening is due to two physically distinct transitions. Indeed, the large difference in the form of χ_{xx} and χ_{zz} indicates that at high temperatures an Ising spin glass forms and at lower temperatures an XY spin glass forms within this glass. The neutron scattering data on $x = 0.50$ confirms the presence of the Ising spin glass, which consists of elongated needlelike clusters. This kind of spin glass where at high temperatures the Ising moments freeze-out then at lower temperatures the XY moments freeze has been theoretically predicted for mixed anisotropy spin glasses.[45]

C. Small-x spin-glass region

Moving to even lower x, the susceptibility evolves continuously towards that of a canonical spin glass, where the features in both real and imaginary susceptibility are analogous to those seen in the canonical spin glasses.[30] Neutron scattering measurements confirm the presence of short-range correlations as are present in spin glasses. Surprisingly, these correlations are antiferromagnetic in nature, not ferromagnetic as could be expected for Ho ions. Mapping the correlations in the scattering plane reveals an ellipsoidal correlation volume with major radius of 44 ± 2 Å along the c axis and minor radius of 13 ± 1 Å along the a axis. The field and temperature dependence of the correlations is consistent with previous studies on spin glasses, where there is a monotonic decrease in intensity as a function of temperature and field.

V. CONCLUSION

To conclude, we have measured the experimental phase diagram of $LiHo_xEr_{1-x}F_4$, finding a rich phase diagram with at least three distinct regions. At large x, the system is a ferromagnet with a low-temperature embedded spin glass. For $x \sim 0.5$, the system likely consists of two coexisting spin glasses, one of which freezes at around 0.5 K and the other at around 0.2 K. At lower x, the features of the spin glass sharpen and by $x = 0.25$ there is only evidence of a single spin-glass state showing antiferromagnetic spin-spin correlations.

ACKNOWLEDGMENTS

We gratefully thank J. Jensen and M. Gingras for fruitful discussions. We thank D. Biner, Bern, for the synthesis of the $LiHo_xEr_{1-x}F_4$ samples. Financial support is gratefully acknowledged from the Swiss SNF, the European Research Council, and DANSCATT of the Danish Agency for Science, Technology, and Innovation. Neutron experiments were performed at the Swiss spallation source (SINQ), Paul Scherrer Institut (PSI), Switzerland, and at Helmholtz-Zentrum Berlin (HZB), Germany.

*julian.piatek@epfl.ch

[1] D. H. Reich, T. F. Rosenbaum, G. Aeppli, and H. J. Guggenheim, Phys. Rev. B **34**, 4956 (1986).
[2] D. H. Reich, B. Ellman, J. Yang, T. F. Rosenbaum, G. Aeppli, and D. P. Belanger, Phys. Rev. B **42**, 4631 (1990).
[3] W. Wu, D. Bitko, T. F. Rosenbaum, and G. Aeppli, Phys. Rev. Lett. **71**, 1919 (1993).
[4] K.-M. Tam and M. J. P. Gingras, Phys. Rev. Lett. **103**, 087202 (2009).
[5] P. E. Hansen, T. Johansson, and R. Nevald, Phys. Rev. B **12**, 5315 (1975).
[6] D. Bitko, T. F. Rosenbaum, and G. Aeppli, Phys. Rev. Lett. **77**, 940 (1996).
[7] H. M. Rønnow, R. Parthasarathy, J. Jensen, G. Aeppli, T. F. Rosenbaum, and D. F. McMorrow, Science **308**, 389 (2005).
[8] H. M. Rønnow, J. Jensen, R. Parthasarathy, G. Aeppli, T. F. Rosenbaum, D. F. McMorrow, and C. Kraemer, Phys. Rev. B **75**, 054426 (2007).
[9] J. Brooke, D. Bitko, T. F. Rosenbaum, and G. Aeppli, Science **284**, 779 (1999).
[10] J. Brooke, T. F. Rosenbaum, and G. Aeppli, Nature (London) **413**, 610 (2001).
[11] S. Ghosh, T. M. Rosenbaum, G. Aeppli, and S. N. Coppersimith, Nature (London) **425**, 48 (2003).
[12] D. M. Silevitch, D. Bitko, J. Brooke, S. Ghosh, G. Aeppli, and T. F. Rosenbaum, Nature (London) **448**, 567 (2007).
[13] S. M. A. Tabei, M. J. P. Gingras, Y.-J. Kao, P. Stasiak, and J.-Y. Fortin, Phys. Rev. Lett. **97**, 237203 (2006).
[14] M. Schechter and N. Laflorencie, Phys. Rev. Lett. **97**, 137204 (2006).
[15] M. J. P. Gingras and P. Henelius, J. Phys.: Conf. Ser. **320**, 012001 (2011).
[16] M. Schechter, Phys. Rev. B **77**, 020401 (2008).
[17] C. Ancona-Torres, D. M. Silevitch, G. Aeppli, and T. F. Rosenbaum, Phys. Rev. Lett. **101**, 057201 (2008).
[18] P. E. Jönsson, R. Mathieu, W. Wernsdorfer, A. M. Tkachuk, and B. Barbara, Phys. Rev. Lett. **98**, 256403 (2007).
[19] J. A. Quilliam, C. G. A. Mugford, A. Gomez, S. W. Kycia, and J. B. Kycia, Phys. Rev. Lett. **98**, 037203 (2007).
[20] J. A. Quilliam, S. Meng, C. G. A. Mugford, and J. B. Kycia, Phys. Rev. Lett. **101**, 187204 (2008).
[21] J. A. Quilliam, S. Meng, and J. B. Kycia, Phys. Rev. B **85**, 184415 (2012).
[22] P. Beauvillain, J.-P. Renard, and P.-E. Hansen, J. Phys. C: Solid State Phys **10**, 709 (1977).
[23] J. Magariño, J. Tuchendler, P. Beauvillain, and I. Laursen, Phys. Rev. B **21**, 18 (1980).
[24] C. Kraemer, N. Nikseresht, J. O. Piatek, N. Tsyrulin, B. Dalla Piazza, K. Kiefer, B. Klemke, T. F. Rosenbaum, G. Aeppli, C. Gannarelli, K. Prokes, A. Podlesnyak, T. Strässle, L. Keller, O. Zaharko, K. W. Krämer, and H. M. Rønnow, Science **336**, 1416 (2012).

[25]S. Fishman and A. Aharony, Phys. Rev. B **18**, 3507 (1978).
[26]S. Fishman and A. Aharony, Phys. Rev. B **19**, 3776 (1979).
[27]S. Fishman and A. Aharony, Phys. Rev. B **21**, 280 (1980).
[28]P.-z. Wong, P. M. Horn, R. J. Birgeneau, C. R. Safinya, and G. Shirane, Phys. Rev. Lett. **45**, 1974 (1980).
[29]P. Wong, P. M. Horn, R. J. Birgeneau, and G. Shirane, Phys. Rev. B **27**, 428 (1983).
[30]J. A. Mydosh, *Spin Glasses: An Experimental Introduction* (Taylor & Francis, London, 1993).
[31]R. Mahendiran, Y. Bréard, M. Hervieu, B. Raveau, and P. Schiffer, Phys. Rev. B **68**, 104402 (2003).
[32]M. K. Singh, W. Prellier, M. P. Singh, R. S. Katiyar, and J. F. Scott, Phys. Rev. B **77**, 144403 (2008).
[33]C. C. Paulsen, S. J. Williamson, and H. Maletta, Phys. Rev. Lett. **59**, 128 (1987).
[34]K. H. Fischer and J. A. Hertz, *Spin Glasses*, edited by D. Edwards and D. Melville (Cambridge University Press, Cambridge, UK, 1991).
[35]A. T. Ogielski, Phys. Rev. B **32**, 7384 (1985).
[36]A. T. Ogielski and I. Morgenstern, Phys. Rev. Lett. **54**, 928 (1985).
[37]B. Barbara, Phys. Rev. Lett. **99**, 177201 (2007).
[38]K. Lefmann, C. Niedermayer, A. Abrahamsen, C. Bahl, N. Christensen, H. Jacobsen, T. Larsen, P. Häfliger, U. Filges, and H. Rønnow, Phys. B (Amsterdam) **385-386**, 1083 (2006).
[39]J. Als-Nielsen, Phys. Rev. Lett. **37**, 1161 (1976).
[40]S. Lovesey, *Theory of Neutron Scattering from Condensed Matter* (Clarendon, Oxford, 1984).
[41]A. Aharony, Phys. Rev. B **8**, 3363 (1973).
[42]S. Ghosh, R. Parthasarathy, T. F. Rosenbaum, and G. Aeppli, Science **296**, 2195 (2002).
[43]A. Biltmo and P. Henelius, Phys. Rev. B **76**, 054423 (2007).
[44]A. Biltmo and P. Henelius, Phys. Rev. B **78**, 054437 (2008).
[45]L. Viana and A. J. Bray, J. Phys. C: Solid State Phys. **16**, 6817 (1983).